



Phase portrait-based stability region estimation for grid-connected VSC with PLL

Yingyi Tang¹  | Yujun Li^{1,2} | Yiyuan Lu¹  | Jiapeng Li^{1,2}

¹School of Electrical Engineering, Xi'an Jiaotong University, Xi'an, China

²Department of Electrical Engineering, The Hong Kong Polytechnic University, Hong Kong, China

Correspondence

Yujun Li, School of Electrical Engineering, Xi'an Jiaotong University, Xi'an, China.
Email: yujunlizju@gmail.com

Funding information

National Natural Science Foundation of China, Grant/Award Number: U2066602

Abstract

Here, the stability region of grid-connected VSC with phase locked loop (PLL) is estimated. First, the conservative stability region is derived via the classical Lyapunov method. Then an energy function is constructed as the general stable condition for the VSC system. Based on the constructed energy function, two estimation methods of the system stability region by approximation of phase trajectory are proposed. The stability regions by the proposed methods are less conservative than that by the classical Lyapunov method. A stability evaluation function for the initial states of the VSC system is further proposed based on the estimated stability region. Time-domain simulations verify the correctness of the proposed methods and the effectiveness of the stability evaluation function.

1 | INTRODUCTION

Facing the dual pressure of the environmental problems and the energy crisis, higher penetration of renewable energies in modern power systems is to be framed in the foreseeable future [1]. Unlike the traditional synchronous generators (SGs), renewable energy generators are interfaced with the power grid via voltage source converters (VSCs) for maximum utilization of wind or solar energy [2]. Generally, the grid-connected VSCs are controlled as grid-following converters where the phase locked loop (PLL) based vector current control (VCC) method is adopted [3]. It has been found that such control dependent synchronizing mechanism may fail when the system is under large disturbances [4] or when the VSC is integrated into very weak ac grids [5], which will greatly challenge the power system stability. It is therefore critical to reveal the instability mechanism and map the stability region of the grid-connected VSC with PLL.

Whether the system would maintain synchronization stability after a given disturbance can be checked by time-domain simulation [6]. System dynamic behaviours are obtained via numerically solving the differential algebraic equations (DAEs) and the system stability can be evaluated by checking whether the state variables approach to a steady state or not. In [7], it is found with time-domain simulations that wind farm might trip off under the severe short-circuit faults since PLL fails

to track the grid phase. Accurate system stability region can be mapped via the repetitive simulations. However, once system topology and operating points change, the system stability region needs to be re-calculated, which is ineffective and time-consuming. Moreover, the system instability mechanism cannot be well explained via simulation studies.

To carry out the synchronization stability analysis of VSC with PLL, a lot of efforts have been devoted into the modelling of grid-connected VSCs. In [8], a unified impedance model of grid-connected VSC is proposed considering the dynamic influences of PLL and current control and the stability impact of PLL and its frequency coupling effect are revealed. However, the second-order PLL model in [8] neglects the non-linear dynamic behaviours of PLL and its instability mechanism cannot be fully investigated. [9–11] focus on developing reduced-order nonlinear models of the system with PLL-based VSC. In [9], a reduced second-order model with high accuracy for the synchronization stability analysis of grid-connected VSC with PLL is proposed. Further, [10] and [11] show that when analyzing the synchronization stability of the PLL-based VSC, the dynamics of the inner current loop can be overlooked since the bandwidth of the PLL is designed much lower than that of the inner current loop.

Lots of stability analysis methods are applied based on the second-order model of PLL-based VSC to reveal the system instability mechanism. The equal area criterion (EAC), which is

This is an open access article under the terms of the [Creative Commons Attribution](https://creativecommons.org/licenses/by/4.0/) License, which permits use, distribution and reproduction in any medium, provided the original work is properly cited.

© 2022 The Authors. *IET Generation, Transmission & Distribution* published by John Wiley & Sons Ltd on behalf of The Institution of Engineering and Technology.

a traditional straightforward method for synchronization stability analysis of SG dominated system, are often considered as an extended approach for the stability analysis of VSC interfaced system [12, 13]. In [14, 15], EAC is applied in the synchronization stability analysis of the VSC with PLL. Ref. [14] provides a clear understanding of the system instability mechanism that synchronization instability may be caused by insufficient equivalent decelerating area. Even though the analytical stability region can be obtained by EAC, the damping effect in the reduced model is overlooked when calculating the maximum deceleration area and its impact on system stability cannot be analyzed by EAC. Ref. [16] points out that the conclusion based on the EAC will be inaccurate when the transient stability effect of the real applicable PLL is fully considered. Moreover, Ref. [17] proposes an improved equal area criterion considering the uncertainty of damping while the derived stability region is rather conservative.

Lyapunov method, on the other hand, is deemed as one effective analytical method to analyze the nonlinear system [18], where the conservative stability region can be derived by constructing proper Lyapunov function. For traditional ac system, [19] has proved that EAC and Lyapunov method are identical for the two-machine system ignoring the damping effect. However, for the stability analysis of the grid-connected VSC with PLL, how to construct a proper Lyapunov function for the second-order model with nonlinear damping term poses a big challenge. In [20], a proper Lyapunov function $V(x)$ is designed for PLL based grid-following VSCs and the stability region is derived. However, the derived stability region is rather conservative for real industry application due to the harsh conditions of the Lyapunov theorem. In [21], the energy function model of the grid-forming and grid-following controlled converters are proposed, and the stability boundary for the grid-following controlled converters is derived under positive damping condition. Yet the system stability when the system state lies inside the negative damping region cannot be evaluated.

Compared with the direct methods of the EAC method and the Lyapunov's method, phase portrait method is an effective method to analyze the second-order nonlinear system. The system state variables are plotted as system trajectory on the phase plane and the system stability can be easily evaluated by checking whether the trajectory deviates the stable equilibrium point (SEP) or not [15, 22]. The impacts of the VSC controller settings on system stability are analyzed in [22] by comparing the phase trajectories of the system under certain disturbances and it is revealed that increasing the damping ratio or the settling time of the PLL can enhance the transient stability of the VSC system. But the critical damping ratio still needs to be obtained via an iterative calculation procedure and the geometric characteristics of system trajectory are not fully considered.

Based on the geometric characteristic of the phase trajectory of grid-connected VSC with PLL, two stability region estimation methods using piece-wise lines to approximate the stable system trajectories are proposed here. The conservation of the proposed estimations is guaranteed since the energy change of stable system trajectories over one cycle is less than that of the constructed curves. Unlike the EAC method that fails to

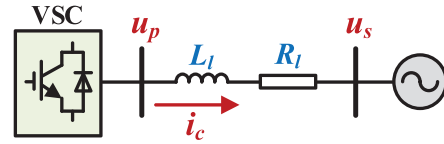


FIGURE 1 Scheme of one VSC connected to the infinite bus

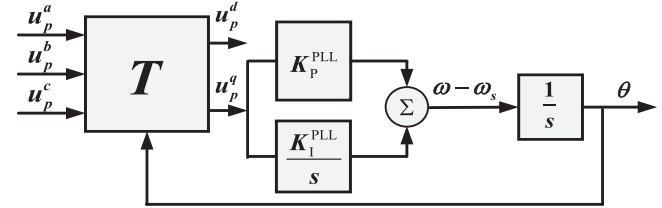


FIGURE 2 Control scheme of PLL

analyze the system damping effect, both the positive damping effect and the negative damping effect of PLL are thoroughly considered by the proposed methods. Accordingly, the stability region derived by the proposed methods is more reliable than that by the EAC method. The derived analytical stability region by the proposed method is proved to be larger than that by Lyapunov method. Then, the energy function-based stability evaluation is further proposed. The effectiveness of the calculation of stable regions and the correctness of the evaluation of system stability are well demonstrated and verified via time-domain simulation results.

2 | SYSTEM MODELLING

As shown in Figure 1, the studied power system consists of one VSC connected to the infinite bus through the transmission line. u_p^{abc} is the voltage of the point of common coupling (PCC) and i_c^{abc} is the current flowing through the converter. R_l and L_l are the line resistance and inductance, respectively. u_s^{abc} is the voltage of the infinite source with the fixed angular speed of ω_s .

2.1 | Dynamic modelling

Normally, the grid-connected VSC relies on PLL to keep the synchronism with the infinite system. As shown in Figure 2, this is achieved by sustaining the q -axis voltage of the PCC as zero during the disturbances. The rotating speed of the dq reference frame is ω , and the d -axis leads u_s^{abc} with the phase of θ . Using the power invariant Park Transformation, u_s^{abc} , u_p^{abc} and i_c^{abc} are transferred in dq -axis reference frame as u_s^{dq} , u_p^{dq} and i_c^{dq} .

$$u_s^d = U_{sL} \cos\theta, \quad u_s^q = -U_{sL} \sin\theta \quad (1)$$

where U_{sL} is the rms value of the line-to-line voltage of u_s^{abc} .

Generally, dynamics of inner current control are much faster than PLL. As a result, when analysing the large disturbance

stability of VSC embedded power system, the state variables of inner current control are reduced to their steady-state values, $i_c^d \equiv i_c^{dref}$, $i_c^q \equiv i_c^{qref}$. Accordingly, the model of the studied system is described as follows.

$$\begin{cases} \frac{d\theta}{dt} = \omega - \omega_s \\ \frac{d\omega}{dt} = K_p^{PLL} \frac{du_p^q}{dt} + K_1^{PLL} u_p^q \end{cases} \quad (2)$$

where,

$$u_p^q - u_s^q = R_l i_c^{qref} + \omega L_l i_c^{dref} \quad (3)$$

Substituting (1) and (3) into (2), the dynamic model of the studied system can be expressed as:

$$\begin{cases} \frac{d\theta}{dt} = \bar{\omega} \\ \frac{d\bar{\omega}}{dt} = \frac{C}{M} - \frac{U_{sL}}{M} \sin\theta - \frac{D(\theta)}{M} \bar{\omega} \end{cases} \quad (4)$$

where,

$$\bar{\omega} = \omega - \omega_s, M = \frac{1 - K_p^{PLL} L_l i_c^{dref}}{K_1^{PLL}}, D(\theta) = C_2 \cos\theta - C_1$$

$$C = \omega_s L_l i_c^{dref} + R_l i_c^{qref}, C_1 = L_l i_c^{dref}, C_2 = \frac{K_p^{PLL}}{K_1^{PLL}} U_{sL}$$

2.2 | Stable equilibrium point of system

One equilibrium point of the final system after large disturbances is obtained from (4).

$$\theta_s = \arcsin \frac{C}{U_{sL}}, \bar{\omega} = 0 \quad (5)$$

Without losing generality, the equilibrium point $(\theta_s, 0)$ is shifted to the origin with a change of variables as follows.

$$x = \theta - \theta_s, y = \bar{\omega} \quad (6)$$

Accordingly, system model (4) is rewritten as:

$$\begin{cases} \frac{dx}{dt} = y \\ \frac{dy}{dt} = -g(x) - f(x)y \end{cases} \quad (7)$$

where,

$$\begin{aligned} g(x) &= -\frac{C}{M} + \frac{U_{sL}}{M} \sin(x + \theta_s), f(x) \\ &= \frac{C_2 \cos(x + \theta_s)}{M} - \frac{C_1}{M} \end{aligned}$$

Equation (7) is the classical Liénard System. Moreover, the term $f(x)$ is considered as the equivalent damping for the system. To ensure the origin as one stable equilibrium point (SEP), small-signal stability of the studied system at the origin should be satisfied. Linearizing the system model of (7) around the origin,

$$\begin{bmatrix} d(\Delta x) / dt \\ d(\Delta y) / dt \end{bmatrix} = \begin{bmatrix} 0 & 1 \\ -g'(0) & -f(0) \end{bmatrix} \begin{bmatrix} \Delta x \\ \Delta y \end{bmatrix} \quad (8)$$

The characteristic function of (8) is obtained as follows:

$$s^2 + f(0)s + g'(0) = 0 \quad (9)$$

Accordingly, the condition that ensures the small signal stability of the origin is derived as follows:

$$f(0) > 0, g'(0) > 0 \quad (10)$$

3 | GENERALIZED ENERGY FUNCTION AND GENERAL STABLE CONDITION

The generalized energy function for system (7) is defined in this section. Then the domain where the defined energy function can be deemed as a Lyapunov function is derived. Then, the general stable condition based on trajectory energy is proposed.

3.1 | Generalized energy function and the domain by Lyapunov's method

One energy function for the second-order Liénard System of (7) is defined as follows:

$$E(x, y) = \frac{y^2}{2} + \int_0^x g(s) ds = F(y) + G(x) \quad (11)$$

where the first term $F(y) = y^2/2$ corresponds to the system kinetic energy and the second term $G(x) = \int_0^x g(s) ds$ relates to the system potential energy.

The generalized energy function in (11) is a natural Lyapunov function candidate for system (7). Clearly, $E(0, 0) = 0$. Based on Lyapunov's second theorem, a domain $D_{Ly} \subset \mathbb{R}^2$ around the origin needs to be defined such that,

$$E(x, y) > 0, \forall (x, y) \in D - \{0\} \quad (12)$$

$$\frac{dE}{dt} = g(x)y + y \cdot [-g(x) - f(x)y] = -f(x)y^2 \leq 0, \quad (13)$$

$$\forall (x, y) \in D$$

Considering that $F(y)$ is always nonnegative, for the integral form $G(x) = \int_0^x g(s)ds$ to be positive definite, there is:

$$xg(x) > 0 \Rightarrow (-\pi - 2\theta_s) < x < (\pi - 2\theta_s) \quad (14)$$

Then in the domain of $\{(x, y) | -\pi - 2\theta_s < x < \pi - 2\theta_s, y \in \mathbb{R}\}$, $E(x, y)$ is ensured to be positive-definite for all $(x, y) \neq (0, 0)$. Moreover, the condition of (13) implies,

$$f(x) \geq 0$$

$$\Rightarrow \left(-\arccos\left(\frac{C_1}{C_2}\right) - \theta_s\right) \leq x \leq \left(\arccos\left(\frac{C_1}{C_2}\right) - \theta_s\right) \quad (15)$$

Namely, in D_{Ly} , the equivalent damping $f(x)$ should be non-negative.

Taking the intersection of the domains in (14) and (15), the domain D_{Ly} is derived as:

$$D_{Ly} = \{(x, y) | x_1 \leq x \leq x_2, y \in \mathbb{R}\} \quad (16)$$

where $x_1 = -\arccos(C_1/C_2) - \theta_s$ and $x_2 = \arccos(C_1/C_2) - \theta_s$.

Accordingly, within the defined domain D_{Ly} , the general energy function $E(x, y)$ is a valid Lyapunov function and by the Lyapunov's second theorem we conclude that the origin is asymptotically stable.

3.2 | General stable condition

Since the system energy is defined in (11), consider one system trajectory \widehat{PQ} from Point $P(x_P, y_P)$ at time t_P to Point $Q(x_Q, y_Q)$ at time t_Q , the energy of Point Q can be calculated by the integration of (13) along \widehat{PQ} :

$$E_Q = E_P + \int_{\widehat{PQ}} \frac{dE(x, y)}{dt} dt = E_P - \int_{t_P}^{t_Q} f(x)y^2 dt \quad (17)$$

where E_P and E_Q are the energy of Point P and Point Q , respectively. Accordingly, the trajectory energy change along \widehat{PQ} is given by:

$$E_{\widehat{PQ}} = E_Q - E_P = - \int_{t_P}^{t_Q} f(x)y^2 dt \quad (18)$$

For any trajectory starting inside the system stability region with an initial energy $E(x, y)$, it will finally converge to the origin and its energy will accordingly approach to zero, $E(0, 0) = 0$. In domain D_{Ly} defined by Lyapunov's method, the trajectory energy is always decreasing based on (13). However, for a trajectory moves in and out of domain D_{Ly} , there is an energy exchange with the trajectory losing energy inside D_{Ly} and gaining energy outside D_{Ly} .

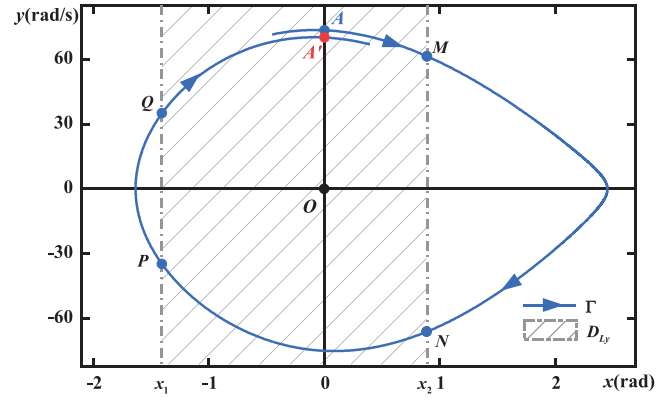


FIGURE 3 System trajectory Γ that overrides D_{Ly}

In fact, as shown in Figure 3, if the net energy change for a trajectory Γ from Point $A(0, y_A)$ to Point $A'(0, y_{A'})$ over one cycle after the quasi-period denoted as T is negative,

$$\int_{t_A}^{t_A+T} \frac{dE}{dt} dt = E_{A'} - E_A = E_{\widehat{AA'}} < 0 \quad (19)$$

then the trajectory Γ is ensured to be inside the actual stability region.

Proof.

$$E_{\widehat{AA'}} = E_{A'} - E_A = \frac{y_{A'}^2}{2} - \frac{y_A^2}{2} < 0 \quad (20)$$

$$\Rightarrow |y_{A'}| < |y_A| \quad (21)$$

Since a trajectory of an autonomous planar system that is not a closed orbit won't intersect, the trajectory Γ is ensured to converge to the origin and the system maintains stable. Accordingly, Γ is identified to be inside the actual stability region. **End**

Divide the energy change in (19) into two parts,

$$\int_{t_A}^{t_A+T} \frac{dE}{dt} dt = \Delta E_+ + \Delta E_- \quad (22)$$

where,

$$\left\{ \begin{aligned} \Delta E_- &= \int_{t_A}^{t_M} [-f(x)y^2] dt + \int_{t_N}^{t_P} [-f(x)y^2] dt \\ &\quad + \int_{t_Q}^{t_A+T} [-f(x)y^2] dt \end{aligned} \right\} < 0$$

$$\Delta E_+ = \left\{ \int_{t_M}^{t_N} [-f(x)y^2] dt + \int_{t_P}^{t_Q} [-f(x)y^2] dt \right\} > 0.$$

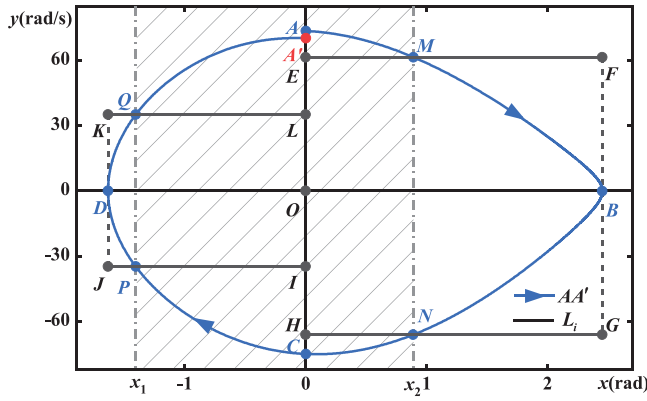


FIGURE 4 Approximation of $\widehat{AA'}$ with horizontal lines

ΔE_+ denotes the increase of the trajectory energy and ΔE_- denotes the decrease of the trajectory energy. In the area of ΔE_- , the equivalent damping $f(x) > 0$ always holds and as for the area of ΔE_+ , $f(x) < 0$. It is indicated that ΔE_- and ΔE_+ denote the positive and negative damping effect on the system stability, respectively. If $\Delta E_- + \Delta E_+ \leq 0$, the total system damping presents positive, and the system is stable.

The condition of (19) reveals the general property of any stable trajectory Γ . Obviously, it does not require the whole trajectory Γ lies inside the positive damping area where $f(x) \geq 0$.

4 | ESTIMATION OF THE DOMAIN SATISFYING THE GENERAL STABLE CONDITION BY TRAJECTORY APPROXIMATION

In order to find the domain satisfying the condition of (19), two estimation methods are proposed by constructing lines L_i to approximate any system trajectory $\widehat{AA'}$ over one cycle. According to the generalized stable condition of (19), if the energy change of the constructed lines L_i satisfies:

$$\int_{\widehat{AA'}} (dE/dt) \cdot dt \leq \sum_{i=1}^n \int_{L_i} (dE/dt) \cdot dt \leq 0 \quad (23)$$

then the approximated trajectory $\widehat{AA'}$ is ensured to be inside the system stability region. Accordingly, the dynamic characteristics of system (7) shown as the geometric properties in its phase portrait are captured by the constructed lines L_i , and the analytical stability domain with less conservation can be derived from:

$$\sum_{i=1}^n \int_{L_i} (dE/dt) \cdot dt = 0 \quad (24)$$

4.1 | Trajectory approximation by horizontal lines

As shown in Figure 4, one system trajectory $\widehat{AA'}$ over one cycle in solid blue is divided into four separated parts, namely arc

\widehat{AMB} , arc \widehat{BNC} , arc \widehat{CPD} , and arc $\widehat{DQA'}$, where Point M , Point N , Point P and Point Q are the four intersect points of the trajectory $\widehat{AA'}$ and the positive damping area $[x_1, x_2]$.

$$x_{M,N} = x_2, \quad x_{P,Q} = x_1, \quad f(x_{M,N,P,Q}) = 0 \quad (25)$$

The energy change for system trajectory $\widehat{AA'}$ over one cycle satisfies,

$$\begin{aligned} E_{\widehat{AA'}} &= E_{A'} - E_A \\ &= E_{\widehat{AMB}} + E_{\widehat{BNC}} + E_{\widehat{CPD}} + E_{\widehat{DQA'}} \end{aligned} \quad (26)$$

We first consider the arc \widehat{AMB} . As demonstrated in Figure 4, one simple horizontal line L_{EF} in black solid is constructed passing Point M to approximated the arc \widehat{AMB} ,

$$L_{EF} : \tilde{y} = y_M \quad (0 < x < x_B) \quad (27)$$

where y_M is value of y for Point M . Point E is the intersect point of L_{EF} and y -axis. Point F is the intersect point of L_{EF} and line $x = x_B$.

Next, we prove that the energy change of arc \widehat{AMB} is less than that of the constructed L_{EF} irrespective of y_M , namely,

$$E_{\widehat{AMB}} < E_{L_{EF}}, \quad \forall y_M \in \mathbb{R} \quad (28)$$

Proof. $E_{\widehat{AMB}}$ can be re-written as:

$$E_{\widehat{AMB}} = E_{\widehat{AM}} + E_{\widehat{MB}} = \int_{\widehat{AM}} \frac{dE}{dt} dt + \int_{\widehat{MB}} \frac{dE}{dt} dt \quad (29)$$

Making substitutions from (13), $E_{\widehat{AM}}$ and $E_{\widehat{MB}}$ in (29) can be expressed as follows based on the relation of $y dt = x$.

$$E_{\widehat{AM}} = - \int_{\widehat{AM}} f(x) y^2 dt = - \int_0^{x_2} f(x) y dx, \quad f(x) > 0 \quad (30)$$

$$E_{\widehat{MB}} = - \int_{\widehat{MB}} f(x) y^2 dt = - \int_{x_2}^{x_B} f(x) y dx, \quad f(x) < 0 \quad (31)$$

The following Inequalities naturally hold.

$$\begin{cases} E_{\widehat{AM}} < -y_M \int_0^{x_2} f(x) dx = E_{L_{EM}} \quad (f(x) > 0) \\ E_{\widehat{MB}} < -y_M \int_{x_2}^{x_B} f(x) dx = E_{L_{MF}} \quad (f(x) < 0) \end{cases} \quad (32)$$

Combining the two Inequalities in (36), the value of $E_{\widehat{AMB}}$ satisfies,

$$\begin{aligned} E_{\widehat{AMB}} &= E_{\widehat{AM}} + E_{\widehat{MB}} \\ &< -y_M \int_0^{x_B} f(x) dx = E_{L_{EM}} + E_{L_{MF}} = E_{L_{EF}} \end{aligned} \quad (33)$$

End

Using the similar technique, Line GH , Line IJ and Line LK are constructed to approximate arc \widehat{BNC} , arc \widehat{CPD} , and arc $\widehat{DQA'}$. As a result, the following inequalities hold.

$$\begin{cases} E_{\widehat{BNC}} < y_N \int_0^{x_B} f(x) dx \\ E_{\widehat{CPD}} < y_P \int_{x_D}^0 f(x) dx \\ E_{\widehat{DQA'}} < -y_Q \int_{x_D}^0 f(x) dx \end{cases} \quad (34)$$

Based on (33) and (34), the value of $E_{\widehat{AA'}}$ satisfies:

$$\begin{aligned} E_{\widehat{AA'}} &= E_{\widehat{AMB}} + E_{\widehat{BNC}} + E_{\widehat{CPD}} + E_{\widehat{DQA'}} \\ &< E_{L_{EF}} + E_{L_{GH}} + E_{L_{IJ}} + E_{L_{LK}} \\ &= (y_N - y_M) \int_0^{x_B} f(x) dx + (y_P - y_Q) \int_{x_D}^0 f(x) dx \end{aligned} \quad (35)$$

Obviously, in (35), $(y_N - y_M) < 0$ and $(y_P - y_Q) < 0$ always hold. Hence, if the following Inequality holds,

$$\int_0^{x_B} f(x) dx \geq 0, \quad \int_{x_D}^0 f(x) dx \geq 0 \quad (36)$$

then the energy change of the constructed lines is negative. As a result, $E_{\widehat{AA'}} < 0$ and $\widehat{AA'}$ is inside the stability region.

The intersect points of the approximated stability system trajectory $\widehat{AA'}$ and the x -axis (namely, Point B and Point D) can be directly obtained based on the condition (24).

$$\int_0^{x_{B,D}} f(x) dx = 0 \Rightarrow x = x_{B,D} \quad (37)$$

Accordingly, the energy change over a cycle for any trajectory within the domain:

$$D_b = \{(x, y) | x_D^b \leq x \leq x_B^b\} \quad (38)$$

is ensured to be negative, where the superscript b denotes the horizontal line approximation method.

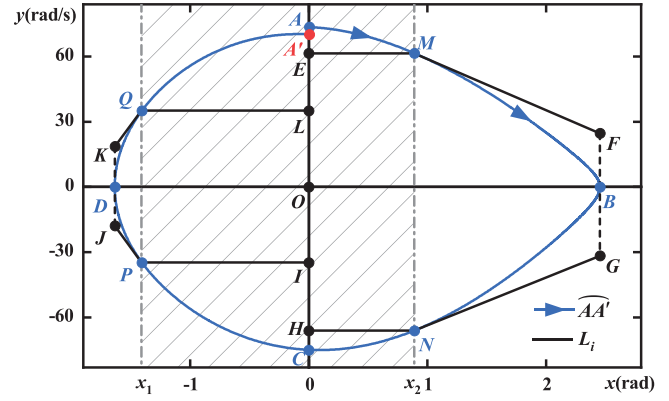


FIGURE 5 Approximation of $\widehat{AA'}$ with tangent lines

4.2 | Trajectory approximation by tangent lines

As shown in Figure 5, one tangent Line MF is utilized to approximate the arc \widehat{MB} instead of the horizontal line such that a larger conservative stability region can be obtained. Point F is the intersection of tangent Line MF and Line $x = x_B$.

The constructed function of Line EM and Line MF is:

$$\tilde{y} = \begin{cases} y_M & (0 < x < x_M) \\ -\frac{g(x_2)}{y_M} (x - x_2) + y_M & (x_2 < x < x_B) \end{cases} \quad (39)$$

where $-g(x_2)/y_M$ is the slope of arc \widehat{MB} at Point M . Due to the convexity of the system trajectory, Line MF is above the arc \widehat{MB} , and it implies,

$$\begin{aligned} E_{\widehat{MB}} &= \int_{x_2}^{x_B} -f(x) y dx \\ &< \int_{x_2}^{x_B} -f(x) \left[-\frac{g(x_2)}{y_M} (x - x_2) + y_M \right] dx \end{aligned} \quad (40)$$

Combining (30) and (40):

$$E_{\widehat{AMB}} < y_M \left[-\int_0^{x_B} f(x) dx + \frac{g(x_2)}{y_M} \int_{x_2}^{x_B} f(x) (x - x_2) dx \right] \quad (41)$$

Due to the negative damping effect in the region of $[x_2, x_B]$, the trajectory energy increases along arc \widehat{MB} . It follows:

$$\begin{aligned} E_M &= \frac{y_M^2}{2} + G(x_2) < E_B = G(x_B) \\ &\Rightarrow y_M^2 < 2 [G(x_B) - G(x_2)] \end{aligned} \quad (42)$$

Moreover, since $f(x) < 0$ within $[x_2, x_B]$,

$$\int_{x_2}^{x_B} f(x)(x-x_2) dx < 0 \quad (43)$$

Based on (42) and (43), it holds that:

$$\begin{aligned} & \frac{g(x_2)}{J_M^2} \int_{x_2}^{x_B} f(x)(x-x_2) dx \\ & < \frac{g(x_2)}{2[G(x_B) - G(x_2)]} \int_{x_2}^{x_B} f(x)(x-x_2) dx \end{aligned} \quad (44)$$

Combining (41) and (44), the value of $E_{\widehat{AMB}}$ satisfies:

$$\begin{aligned} E_{\widehat{AMB}} & < \left[y_M - \int_0^{x_B} f(x) dx \right. \\ & \left. + \frac{g(x_2)}{2[G(x_B) - G(x_2)]} \int_{x_2}^{x_B} f(x)(x-x_2) dx \right] \end{aligned} \quad (45)$$

Using the similar technique, the horizontal Line GN and the tangent Line LH are constructed to approximate the arc \widehat{BNC} . According to (41), the following Inequality holds,

$$E_{\widehat{BNC}} < J_N \left[- \int_{x_B}^0 f(x) dx + \frac{g(x_2)}{J_N^2} \int_{x_B}^{x_2} f(x)(x-x_2) dx \right] \quad (46)$$

Considering that the energy of Point N can be calculated from the energy of Point B ,

$$E_N = E_B - \int_{x_B}^{x_N} f(x)y dx \quad (47)$$

the following Inequalities are derived.

$$\begin{aligned} & \frac{J_N^2}{2} + G(x_N) > G(x_B) - J_N \int_{x_B}^{x_N} f(x) dx \\ & \Rightarrow J_N^2 + 2 \left[\int_{x_B}^{x_N} f(x) dx \right] J_N + 2[G(x_2) - G(x_B)] > 0 \\ & \Rightarrow J_N \langle k_N \langle 0 \Rightarrow J_N^2 \rangle k_N^2 \rangle > 0 \end{aligned} \quad (48)$$

where,

$$\begin{aligned} k_N & = \int_{x_2}^{x_B} f(x) dx \\ & - \sqrt{\left[\int_{x_2}^{x_B} f(x) dx \right]^2 + 2[G(x_B) - G(x_2)]} \end{aligned}$$

Substituting the J_N^2 in (46) with k_N^2 ,

$$E_{\widehat{BNC}} < J_N \left[- \int_{x_B}^0 f(x) dx + \frac{g(x_2)}{k_N^2} \int_{x_B}^{x_2} f(x)(x-x_2) dx \right] \quad (49)$$

Obviously,

$$k_N^2 > 2[G(x_B) - G(x_2)]$$

Combing (45) and (49), the energy change over the right part of the system trajectory denoted as $E_{\widehat{ABC}}$ satisfies,

$$\begin{aligned} E_{\widehat{ABC}} & = E_{\widehat{AMB}} + E_{\widehat{BNC}} \\ & < (y_M - y_N) \left[\int_{x_B}^0 f(x) dx + \frac{g(x_2)}{k_N^2} \int_{x_2}^{x_B} f(x)(x-x_2) dx \right] \end{aligned} \quad (50)$$

Similarly, the energy change over the left part of the system trajectory denoted as $E_{\widehat{CDA}'}$ satisfies,

$$\begin{aligned} E_{\widehat{CDA}'} & = E_{\widehat{CPD}} + E_{\widehat{DQA}'} \\ & < (y_Q - y_P) \left[\int_0^{x_D} f(x) dx + \frac{g(x_1)}{k_Q^2} \int_{x_D}^{x_1} f(x)(x-x_1) dx \right] \end{aligned} \quad (51)$$

where,

$$0 < y_Q < k_Q$$

$$k_Q = \int_{x_1}^{x_D} f(x) dx + \sqrt{\left[\int_{x_D}^{x_1} f(x) dx \right]^2 + 2[G(x_D) - G(x_1)]}$$

According to (50) and (51), if the following Inequalities hold:

$$\begin{cases} \left[\int_0^{x_B} f(x) dx - \frac{g(x_2)}{k_N^2} \int_{x_2}^{x_B} f(x)(x-x_2) dx \right] \geq 0 \\ \left[\int_{x_D}^0 f(x) dx - \frac{g(x_1)}{k_Q^2} \int_{x_D}^{x_1} f(x)(x-x_1) dx \right] \geq 0 \end{cases} \quad (52)$$

Then $E_{\widehat{AA}'} < 0$ and trajectory \widehat{AA}' is inside the stability region.

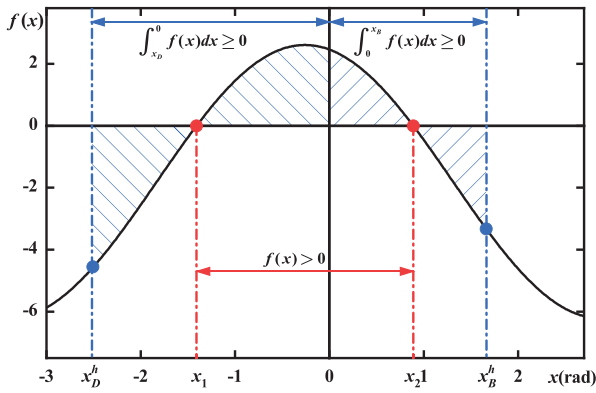


FIGURE 6 Stability regions by Lyapunov method and horizontal line approximation

Therefore, the derived analytical conservative domain satisfying the condition of (19) is obtained as:

$$\int_0^{x_{B,D}} f(x) dx - \frac{g(x_2)}{k_N^2} \int_{x_2}^{x_{B,D}} f(x) (x - x_2) dx = 0 \quad (53)$$

$$\Rightarrow x = x_{B,D}$$

Similarly, the energy change over a cycle for any trajectory within the domain:

$$D_t = \{(x, y) | x_D^t \leq x \leq x_B^t\} \quad (54)$$

is ensured to be negative, where the superscript t denotes the tangent line approximation method.

4.3 | Comparison of D_{L_y} , D_h and D_t

The domain $D_{L_y} = \{(x, y) | x_1 \leq x \leq x_2\}$ by Lyapunov's method requires the equivalent damping $f(x)$ to be positive. As shown in Figure 6, this requirement is relaxed by the proposed horizontal line approximation method. In the domain of $D_b = \{(x, y) | x_D^b \leq x \leq x_B^b\}$, only the total damping effect, namely the integral of $f(x)$ over a cycle, is required to be positive.

$$f(x) \geq 0 \Rightarrow \begin{cases} \int_0^{x_B} f(x) dx \geq 0 \\ \int_{x_D}^0 f(x) dx \geq 0 \end{cases} \quad (55)$$

Accordingly, the derived region D_b is less conservative than D_{L_y} , namely, $D_{L_y} \subset D_b$.

Moreover, since:

$$-\frac{g(x_2)}{k_N^2} \int_{x_2}^{x_B} f(x) (x - x_2) dx > 0,$$

$$-\frac{g(x_1)}{k_Q^2} \int_{x_D}^{x_1} f(x) (x - x_1) dx > 0$$

always hold, it follows:

$$\begin{cases} \int_0^{x_B} f(x) dx \geq 0 \\ \int_{x_D}^0 f(x) dx \geq 0 \end{cases} \quad (56)$$

$$\Rightarrow \begin{cases} \int_0^{x_B} f(x) dx - \frac{g(x_2)}{k_N^2} \int_{x_2}^{x_B} f(x) (x - x_2) dx \geq 0 \\ \int_{x_D}^0 f(x) dx - \frac{g(x_1)}{k_Q^2} \int_{x_D}^{x_1} f(x) (x - x_1) dx \geq 0 \end{cases}$$

Accordingly, the region D_t by tangent line approximation method further reduces the conservation of D_b .

5 | STABILITY REGION ESTIMATION BY THE GENERALIZED ENERGY FUNCTION

Based on the generalized energy function, the actual system stability region is estimated in this section using the domain D_{L_y} by Lyapunov's method and the domain D_b and D_t by the proposed trajectory approximation methods.

5.1 | Stability region estimation with Lyapunov's method

Denote the actual stability region of the origin for system (7) as R_A . It should be noted that D_{L_y} is not an estimate of R_A since D_{L_y} is unbounded. Using LaSalle's Theorem, one Lyapunov surface Ω_{L_y} , which is a compact positively invariant subset of D_{L_y} , is chosen as an estimate of R_A .

$$\Omega_{L_y} = \{x, y \in \mathbb{R} | E(x, y) \leq E(x_2, 0)\} \quad (57)$$

where $E(x_2, 0)$ is the defined generalized trajectory energy of Point $(x_2, 0)$. It can be seen that once the value of energy surface $E(x_2, 0)$ is rather small, the estimate Ω_{L_y} will be too conservative for realistic application.

5.2 | Stability region estimation with trajectory approximation

A trajectory initially starting from the region of $D_{b,t} = \{x, y \in \mathbb{R} | x_D \leq x \leq x_B\}$ might move from one energy surface $E(x, y) = e_1$ to a higher energy surface $E(x, y) = e_2$ where $e_2 > e_1$ since D_b or D_t consists the negative damping area. This problem does not arise when the stability region is estimated by a compact positively invariant subset of $D_{b,t}$; that is, a compact set $\Omega \subset D_{b,t}$ such that every trajectory starting in Ω stays in Ω .

for all future time. The simplest such estimation is the set:

$$\Omega = \{ (x, y) \in D_{b,t} \mid E(x, y) \leq c \} \quad (58)$$

Normally, the disturbances or the initial values for the studied dynamic system appear in the first quadrant in the phase plane. Therefore, the estimate of the actual stability region is chosen as:

$$\Omega = \left\{ x \in [0, x_B] \mid E(x, y) \leq \tilde{E} \right\} \quad (59)$$

where the energy boundary \tilde{E} can be derived from the minimal energy of the system over the region $[0, x_B]$.

According to (13), the minimal energy in the first quadrant of the phase plane is the energy of Point M . Since

$$\begin{aligned} E_M &= \frac{y_M^2}{2} + G(x_2) = G(x_B) + \int_{x_2}^{x_B} f(x) y dx \\ &> G(x_B) + y_M \int_{x_M}^{x_B} f(x) dx \end{aligned} \quad (60)$$

It implies:

$$y_M > k_M > 0 \quad (61)$$

where,

$$\begin{aligned} k_M &= \int_{x_B}^{x_2} f(x) dx \\ &+ \sqrt{\left[\int_{x_2}^{x_B} f(x) dx \right]^2 + 2[G(x_B) - G(x_2)]} \end{aligned} \quad (62)$$

Combing (60) and (61):

$$E_M > k_M^2 + G(x_2) \quad (63)$$

Accordingly, the energy boundary in (59) is chosen as:

$$\tilde{E} = \frac{k_M^2}{2} + G(x_2) \quad (64)$$

It should be noted that the k_M in (62) is a function of x_B obtained from (37) or (53), and as a result, the energy boundary \tilde{E} is calculated by x_B^b or x_B^f .

$$\begin{aligned} \tilde{E}_{x_B^b} &= \frac{1}{2} k_M^2 \Big|_{x_B^b} + G(x_2) \\ \text{or } \tilde{E}_{x_B^f} &= \frac{1}{2} k_M^2 \Big|_{x_B^f} + G(x_2) \end{aligned} \quad (65)$$

Moreover, the stability of the system can be judged without further point-to-point calculations of the swing curves. If the

energy of the final system state is less than \tilde{E} , then system is ensured to maintain stability. The stability region estimation and the stability judgment by the proposed method is demonstrated in Figure 7.

6 | VALIDATION AND CASE ANALYSIS

To validate the stability regions by the proposed estimation methods, the case of one VSC connected to the infinite bus through transmission line is applied. The voltage of infinite source U_{sL} is 110 kV and other related parameters for the case study are listed in Table 1. The large disturbances applied in the case study are set as the infinite source U_{sL} suddenly dropping to 0.3 p.u. at time $t_f = 0.01s$ and returning to U_{sL} after t_c seconds.

6.1 | Comparison of the boundary x_2 , x_B^b and x_B^f

In the first quadratic of the phase plane, the boundary $x = x_2$ by Lyapunov's method and the boundaries $x = x_B^b$ and $x = x_B^f$ by the proposed trajectory approximation methods are calculated with different PI settings of PLL. The calculation results are shown in Tables 2 and 3. For comparison, the exact stability boundary $x = x_B^e$ obtained by increasing t_c until the simulation shows the instability is also listed in Tables 2 and 3.

Take the case of $K_p^{\text{PLL}} = 0.10$, $K_i^{\text{PLL}} = 20$ for elaboration, where $\theta_s = 0.3697$ rad, the system trajectories with different fault duration time are plotted in Figure 8a–c. It can be seen from Figure 8a that the trajectory in solid black with $t_c = 55.9$ ms is inside the stability boundary $x = x_2 = 0.9689$ rad by Lyapunov's method and the system stability is maintained. With the increase of the fault duration time, the trajectories shown in Figure 8b override the positive damping area (the shaded area) and still converge to the origin.

It can be seen that the trajectory in solid blue with $t_c = 82.4$ ms is within the boundary of $x = x_B^b = 1.8617$ rad (blue dashed line) and the trajectory in solid red with $t_c = 84.9$ ms is within the boundary of $x = x_B^f = 2.0365$ rad (red dashed line), verifying the correctness of the two proposed phase portrait based estimation methods well. It also shows that the proposed methods can highly reduce the conservativeness of Lyapunov's method since the estimated boundary by the horizontal line approximation method (x_B^b) is almost twice as much as the region by the direct method of Lyapunov (x_2).

In Figure 8c the trajectory in solid yellow with $t_c = 86.9$ ms reaches the exact stability boundary $x = x_B^e = 2.3404$ rad (yellow dashed line). While with $t_c = 87.0$ ms, the trajectory in solid green overrides the boundary of $x = x_B^e$ and the system is unstable. It should be noticed that the tangent line estimation (x_B^f) further improves the horizontal line estimation (x_B^b) by 0.1–0.2 rads. That is because the constructed approximation lines by the tangent line method vary with the slope of the actual trajectories and as a result, x_B^f is closer to the exact boundary x_B^e than x_B^b .

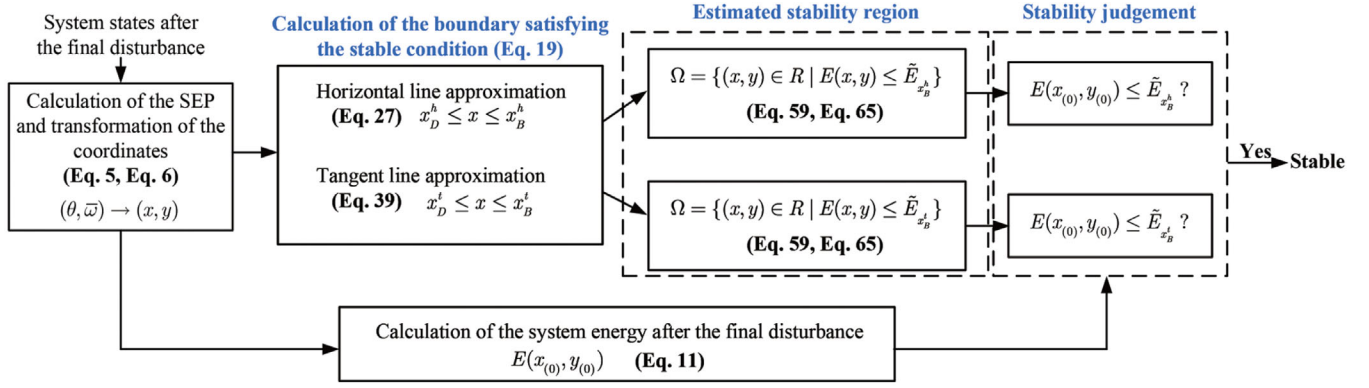


FIGURE 7 The block diagram of the proposed method

TABLE 1 Parameters of the grid-connected VSC

Symbol	Item	Value
U_B	Base value of ac line voltage	110 (kV)
S_B	Base capacity of system	100 (MVA)
L_l	Inductance of transmission line	0.5 (p.u.)
R_l	Resistance of transmission line	0.05 (p.u.)
ω_s	Fixed system angular speed	100π (rad/s)
i_c^{dref}	d -axis current reference	0.6570 (kA)
i_c^{qref}	q -axis current reference	0 (kA)

6.2 | Energy boundaries by Lyapunov's method and the proposed method

The energy boundaries by $E(x_2, 0)$, $\tilde{E}_{x_B^h}$ and $\tilde{E}_{x_B^t}$ with different control parameters of PLL are calculated and listed in Tables 4 and 5.

Take the case of $K_p^{PLL} = 0.10$, $K_I^{PLL} = 20$ for elaboration. Figure 9 shows the energy change of the system trajectories with respect to time. The energy boundary $E(x_2, 0) = 784.9$ by Lyapunov's method is plotted as the black dashed line in

Figure 9a. $\tilde{E}_{x_B^h} = 2174.2$ by horizontal line approximation and $= 2441.7$ by tangent line approximation are plotted as the blue dashed line and the red dashed line in Figure 9b, respectively. It can be seen that under $t_c = 55.9$ ms (solid black), the energy of Point $S_1(781.422)$ is within the boundary $E(x_2, 0)$ and the system trajectory energy is monotonically decreasing with respect to time, ensuring the system stability. It verifies the effectiveness of $E(x_2, 0)$ in (57), showing that when the system energy is less than the Lyapunov's energy boundary after the final disturbance, the system trajectory will be kept in the positive damping area and the system energy will monotonically decrease to zero.

As for $t_c = 82.4$ ms (solid blue), the energy of Point $S_2(1882.3)$ exceeds $E(x_2, 0)$ and is still within $\tilde{E}_{x_B^h}$, showing the conservativeness of the judgement by Lyapunov's method. Meanwhile, it matches well with the result in Figure 8b that the trajectory in solid blue is within the boundary $x = x_B^h$, verifying the effectiveness of stability energy boundary $\tilde{E}_{x_B^h}$. Similarly, with $t_c = 84.9$ ms (solid red), the energy of Point $S_3(2000.2)$ exceeds $\tilde{E}_{x_B^h}$ and is within the range of $\tilde{E}_{x_B^t}$. It can be seen that in this case, both the Lyapunov's method and the horizontal line method fail to judge the system stability, while the tangent line

TABLE 2 Values of the estimated and the exact stability boundaries under the different K_p^{PLL}

Control Parameters $K_p^{PLL} (K_I^{PLL} = 20)$	Lyapunov's method x_2	Proposed method x_B^h, x_B^t		Exact boundary x_B^e
0.03	0.3272	0.6158	0.6557	1.2442
0.10	0.9689	1.8617	2.0365	2.3404
0.17	1.0653	2.0746	2.2545	2.3738

TABLE 3 Values of the estimated and the exact stability boundaries under the different K_I^{PLL}

Control Parameters $K_I^{PLL} (K_p^{PLL} = 0.10)$	Lyapunov's method x_2	Proposed method x_B^h, x_B^t		Exact boundary x_B^e
30	0.8488	1.6109	1.7461	2.3726
40	0.7230	1.3605	1.4642	2.3768
50	0.5883	1.1019	1.1795	2.1109

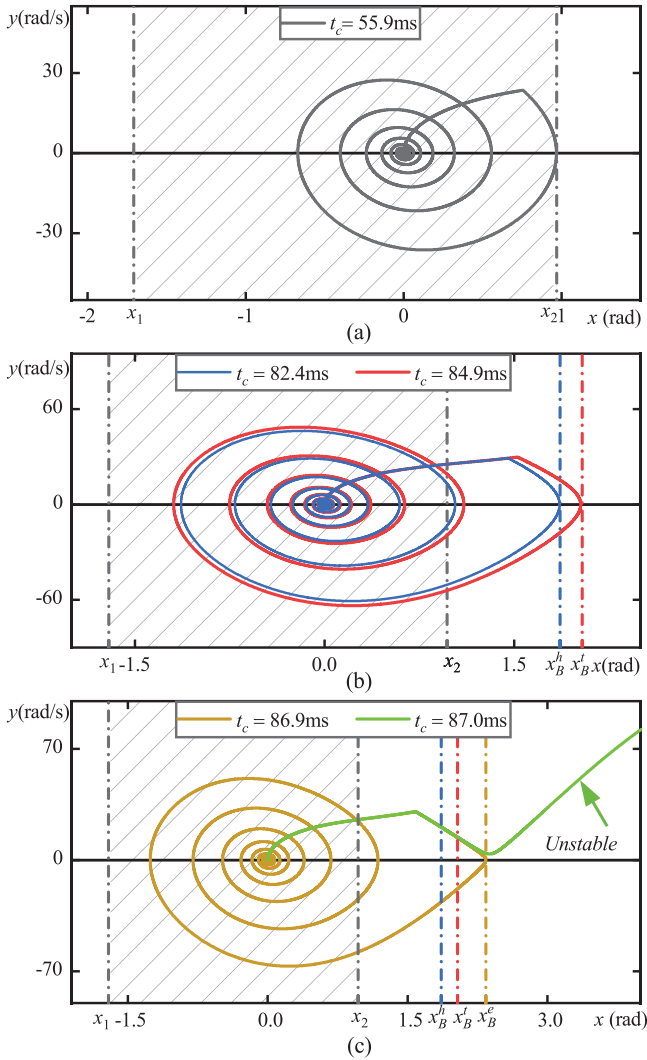


FIGURE 8 System trajectories with different fault duration time

TABLE 4 Values of the estimated energy boundaries under the different K_p^{PLL}

Control parameters	Lyapunov's method	Proposed method	
		$\tilde{E}_{x_B^h}$	$\tilde{E}_{x_B^l}$
$K_p^{\text{PLL}} (K_I^{\text{PLL}} = 20)$	$E(x_2, 0)$		
0.03	104.6	349.9	393.4
0.10	784.9	2174.2	2441.7
0.17	926.6	2684.4	3034.2

TABLE 5 Values of the estimated energy boundaries under the different K_I^{PLL}

Control parameters	Lyapunov's method	Proposed method	
		$\tilde{E}_{x_B^h}$	$\tilde{E}_{x_B^l}$
$K_I^{\text{PLL}} (K_p^{\text{PLL}} = 0.10)$	$E(x_2, 0)$		
30	938.0	2690.0	3023.1
40	940.6	2803.6	3151.4
50	806.1	2501.3	2811.4

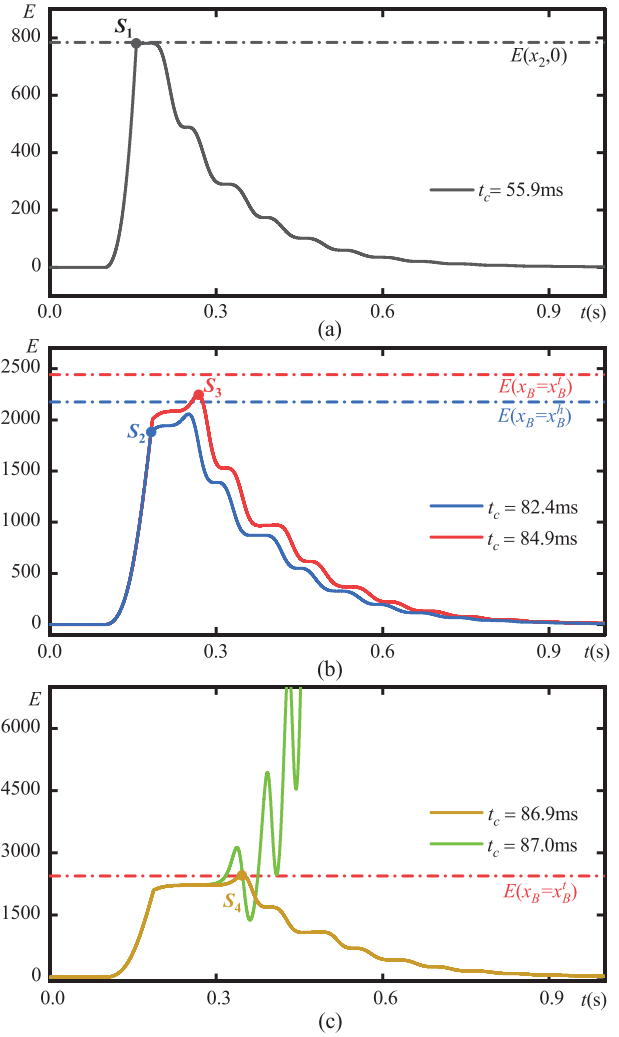


FIGURE 9 Trajectory energy with different fault duration time

method can still tell that the system would maintain stable. It is again proved the conservativeness of the Lyapunov's method and the horizontal line approximation method.

In Figure 9c, with the critical fault duration time $t_c = 86.9$ ms (solid yellow), the energy decreasing property still holds even though the energy of Point S_4 (2095.2) exceeds $\tilde{E}_{x_B^l}$, verifying the conservativeness of the tangent line approximation method. It can be seen that with $t_c = 87.0$ ms, the system energy crosses the energy boundary and increases rapidly to the infinite as shown the solid green line in Figure 9c.

7 | CONCLUSION

Here, two estimation methods based on approximating the system trajectories according to their geometric property are proposed and verified. Moreover, the derived analytical stable regions by the two proposed methods are proved to be larger than that by Lyapunov method. The conservation of the derived system stable region is guaranteed since the energy change of

stable system trajectories over one cycle is less than that of the constructed curves. The evaluation result can be applied in the early-stage stability analysis of grid-connected VSC system with PLL.

AUTHOR CONTRIBUTIONS

Y.T.: Conceptualization; Validation; Writing – original draft; Writing – review and editing. Y.Li.: Conceptualization; Methodology; Project administration; Supervision; Writing – original draft; Writing – review and editing. Y.Lu.: Software; Validation; Visualization; Writing – review and editing. J.L.: Validation; Writing – review and editing.

ACKNOWLEDGEMENTS

This work is supported by the National Natural Science Foundation of China under Grant U2066602.

CONFLICT OF INTEREST

The authors declare no conflict of interest.

DATA AVAILABILITY STATEMENT

The data that support the findings of this study are available from the corresponding author upon reasonable request.

ORCID

Yingyi Tang  <https://orcid.org/0000-0002-8701-5971>

Yiyuan Lu  <https://orcid.org/0000-0002-5514-9000>

REFERENCES

- Hatziargyriou, N., Milanovic, J., Rahmann, C., et al.: Definition and classification of power system stability—Revisited and extended. *IEEE Trans. Power Syst.* 36(4), 3271–3281 (2021)
- Wen, B., Dong, D., Boroyevich, D., et al.: Impedance-based analysis of grid-synchronization stability for three-phase paralleled converters. *IEEE Trans. Power Electron.* 31(1), 26–38 (2016)
- Huang, L., Wu, C., Zhou, D., et al.: A double-pll-based impedance reshaping method for extending stability range of grid following inverter under weak grid. *IEEE Trans. Power Electron.* 37(4), 4091–4104 (2022)
- Goksu, O., Teodorescu, R., Bak, C.L., et al.: Instability of wind turbine converters during current injection to low voltage grid faults and PLL frequency based stability solution. *IEEE Trans. Power Syst.* 29(4), 1683–1691 (2014)
- Davari, M., Mohamed, A.: Robust vector control of a very weak-grid-connected voltage-source converter considering the phase-locked loop dynamics. *IEEE Trans. Power Electron.* 32(2), 977–994 (2016)
- Huang, M., Peng, Y., Tse, C.K., et al.: Bifurcation and large-signal stability analysis of three-phase voltage source converter under grid voltage dips. *IEEE Trans. Power Electron.* 32(11), 8868–8879 (2017)
- Ma, S., Geng, H., Liu, L., et al.: Grid-synchronization stability improvement of large scale wind farm during severe grid fault. *IEEE Trans. Power Syst.* 33(1), 216–226 (2018)
- Wang, X., Harnefors, L., Blaabjerg, F.: Unified impedance model of grid-connected voltage-source converters. *IEEE Trans. Power Electron.* 33(2), 1775–1787 (2018)
- Taul, M.G., Wang, X., Davari, P., et al.: An efficient reduced-order model for studying synchronization stability of grid-following converters during grid faults. In: 2019 20th Workshop on Control and Modeling for Power Electronics (COMPEL), Toronto, ON, Canada, pp. 1–7 (2019)
- Harnefors, L., Wang, X., Yepes, A.G., et al.: Passivity-based stability assessment of grid-connected vscs—An overview. *IEEE J. Emerging Sel. Top. Power Electron.* 4(1), 116–25 (2016)
- He, X., Geng, H., Ma, S., et al.: Transient stability analysis of grid-tied converters considering PLL's nonlinearity. *CPSS Trans. Power Electron. Appl.* 4(1), 40–49 (2019)
- He, X., Geng, H., Xi, J., et al.: Resynchronization analysis and improvement of grid-connected VSCs during grid faults. *IEEE J. Emerging Sel. Top. Power Electron.* 9(1), 438–450 (2021)
- Wu, H., Wang, X.: Transient angle stability analysis of grid-connected converters with the first-order active power loop. In: 2018 IEEE Applied Power Electronics Conference and Exposition (APEC), San Antonio, TX, USA, pp. 3011–3016 (2018)
- Hu, Q., Fu, L., Ma, F., et al.: Large signal synchronizing instability of PLL-based VSC connected to weak AC grid. *IEEE Trans. Power Syst.* 34(4), 3220–3229 (2019)
- Andrade, F., Kampouropoulos, K., Romeral, L., et al.: Study of large-signal stability of an inverter-based generator using a Lyapunov function. In: IECON 2014 - 40th Annual Conference of the IEEE Industrial Electronics Society, Dallas, TX, USA, pp. 1840–1846 (2014)
- Wu, H., Wang, X.: Transient stability impact of the phase-locked loop on grid-connected voltage source converters. In: 2018 International Power Electronics Conference (IPEC-Niigata 2018 -ECCE Asia), Niigata, Japan, pp. 2673–2680 (2018)
- Tang, Y., Tian, Z., Zha, X., et al.: An improved equal area criterion for transient stability analysis of converter-based microgrid considering nonlinear damping effect. *IEEE Trans. Power Electron.* 37(9), 11272–11284 (2022)
- Shuai, Z., Shen, C., Liu, X., et al.: Transient angle stability of virtual synchronous generators using lyapunov's direct method. *IEEE Trans. Smart Grid* 10(4), 4648–4661 (2019)
- Gless, G.E.: Direct method of liapunov applied to transient power system stability. *IEEE Trans. Power Apparatus Syst.* PAS-85(2), 159–168 (1966)
- Mansour, M.Z., Me, S.P., Hadavi, S., et al.: Nonlinear transient stability analysis of phased-locked loop-based grid-following voltage-source converters using lyapunov's direct method. *IEEE J. Emerging Sel. Top. Power Electron.* 10(3), 2699–2709 (2022)
- Fu, X., Sun, J., Huang, M., et al.: Large-signal stability of grid-forming and grid-following controls in voltage source converter: A comparative study. *IEEE Trans. Power Electron.* 36(7), 7832–7840 (2021)
- Wu, H., Wang, X.: Design-oriented transient stability analysis of PLL synchronized voltage-source converters. *IEEE Trans. Power Electron.* 35(4), 3573–3589 (2020)

How to cite this article: Tang, Y., Li, Y., Lu, Y., Li, J.: Phase portrait-based stability region estimation for grid-connected VSC with PLL. *IET Gener. Transm. Distrib.* 17, 730–741 (2023). <https://doi.org/10.1049/gtd2.12701>